Over-the-air Array Calibration of mmWave Phased Array in Beam-steering Mode Based on Measured Complex Signals

Wang, Zhengpeng ; Zhang, Fengchun; Gao, Huaqiang; Franek, Ondrej; Pedersen, Gert Frølund; Fan, Wei

Published in:
I E E E Transactions on Antennas and Propagation

DOI (link to publication from Publisher):
10.1109/TAP.2021.3076349

Publication date:
2021

Document Version
Accepted author manuscript, peer reviewed version

Over-the-air Array Calibration of mmWave Phased Array in Beam-steering Mode Based on Measured Complex Signals

Zhengpeng Wang, Fengchun Zhang, Huaqiang Gao, Ondrej Franek, Gert F. Pedersen and Wei Fan

***Abstract*—Accurate knowledge of initial complex excitation coefficients for phased array elements is essential to ensure accurate array performance. In the literature, many array calibration algorithms have been proposed for this purpose, which generally require customized phase setting for individual phase shifters connected to array elements. In this paper, a new array calibration method is proposed for phased array operating in beam-steering mode only. That is, phase shifts of elements are only simultaneously set according to the beam-steering directions and therefore there is no need for dedicated individual element phase tuning. The proposed method requires minimum number of complex-signal measurements in principle, which enables fast measurement. Furthermore, it is found that the performance of the proposed method is determined by the beam steering matrix, whose condition number is mainly ruled by the beam-steering angle interval. The proposed method is numerically simulated and experimentally validated in a millimeter-wave (mmWave) phased array antenna-in-package (AiP) platform at 28 GHz. The proposed method presents good agreement with the well-known rotating element electric field vector (REV) array calibration method, with an amplitude error and phase error within $\pm$0.5 dB and $\pm 5^o$, respectively. Furthermore, the reconstructed array pattern with the proposed method offers excellent match with the measured array pattern.**

***Index Terms*—Over-the-air test, millimeter-wave phased array, array calibration, beam-steering, in-situ antenna measurement, antenna-in-package (AiP)**

I. Introduction

The demand for ever-increasing data-rate for data-intensive applications has motivated great interest in millimeter-wave (mmWave) bands and beyond, which offer large available bandwidths [1]–[5]. mmWave systems have found wide applications in satellite communication, radar and the fifth generation (5G) radios. The large available bandwidths and reduced physical size at high frequencies make mmWave antenna systems attractive. However, the benefits are offset to some extent by high propagation loss and low signal-to-noise ratio (SNR) at mmWave frequencies [6]. Antenna-in-package (AiP) technology, which integrates antenna systems with radio transceiver circuits into a single package, is the current mainstream solution for mmWave radios and radars. AiP technology enables low lossy and low-cost integration systems for mmWave systems [7].

Phased array antenna systems, where each of array elements is fed by a complex excitation coefficient, have found wide applications in the mmWave systems, e.g. beamforming for directional signal transmission or reception, nulling for interference suppression, beam-steering to track dominant propagation paths, and plane-wave generator (PWG) to synthesize a plane wave in the proximity of the PWG array [8]–[10]. The phased array performance demands precise control of the amplitude and phase excitation of the array elements. Therefore, exact knowledge of the amplitude and phase excitation is essential. However, initial complex excitation coefficients among array elements might differ in practical phased array systems, due to component characteristics drift over temperature and age. Furthermore, radio frequency (RF) impairments, e.g. uncertainty of the attenuator and phase shifter control network, would introduce inhomogeneities among phased array RF branches as well. The objective of array calibration is to obtain the complex excitation coefficients (amplitude and phase) of the individual antenna elements and possibly to compensate the element-to-element inhomogeneities (i.e. to ensure that the signal path to each element is identical). The array calibration is essential to maintain an acceptable beamforming performance since the complex excitation difference among array elements might increase over temperature, humidity and age. In [11], the antenna array is calibrated by injecting identical tones directly into the array receiver ports and measuring the transfer functions of all paths. However, individual element ports might be not accessible for some phased arrays due to their highly integrity and compact structures. Therefore, it is desirable that array calibration should be performed in over-the-air radiated mode, i.e., without access to the antenna element ports.

One popular and simple strategy adopted in the industry is the single-element measurement, where the response of individual elements are sequentially determined with only a single element activated. This typically requires on-off operation of the phased array (i.e. with the illuminated element enabled and other elements properly terminated) and the help of an accurate near-field scanner [12], [13]. However, for mmWave phased array AiP, this strategy requires high repositioning precision of the near field scanner system (which leads to high system cost), and precise knowledge of the AiP antenna configuration (which precludes application for "black-box" AiPs). Furthermore, factors such as transceiver module variations,

Zhengpeng Wang is with Electronics and Information Engineering, Beihang University, Beijing 100191, China.

Fengchun Zhang, Huaqiang Gao, Ondrej Franek, Gert F. Pedersen and Wei Fan are with the Antenna Propagation and Millimeter-wave Systems (APMS) section, Aalborg University, Denmark.

Huaqiang Gao is also with the Beijing Key Laboratory of Work Safety Intelligent Monitoring, Department of Electronic Engineering, Beijing University of Posts and Telecommunications, Beijing 100876, China.

Corresponding author: Wei Fan (Email: wfa@es.aau.dk).

mutual coupling, and influence of antenna structures cannot be considered in the single-element measurement [14].

In general, a phased array is designed to work in an "all-on" mode, i.e., with all elements radiating simultaneously, to electrically steer beams or nulls to the desired directions. The element-to-element inhomogeneities in the "all-on" mode and "on-off" mode might be different due to non-negligible mutual coupling effect between elements. Hence, the phased array calibration performed in the "all-on" mode is more reasonable and accurate for practical phased arrays [15]. Some simultaneous measurement methods based on orthogonal encoded signals are proposed in [16], [17]. These methods might not work for commercial user equipments (UEs), where the transmitted signals from the UEs can not be designed (known). Below, we focus on more general calibration methods applicable for phased arrays only required phase tuning ability.

One effective calibration method is the so-called rotating element electric field vector (REV) method [18]. The basic principle is that the array power variation is measured while the phase of a single element is successively tuned from 0^o to 360^o, and the complex excitation of the corresponding element can be determined. The REV procedure does not require any phase measurements and has been widely applied to many applications. Several methods were also proposed to improve measurement speed and accuracy based on the REV principle [14], [16], [19]–[24]. Besides the amplitude-only measurements, the complex signal (i.e. both amplitude and phase) measurement methods were applied as well for array calibration [25], [26]. Compared to amplitude-only methods, fewer number of measurements are typically required. However, all available "all-on" mode calibration methods (i.e. both the amplitude-only and complex signal measurements) in the literature generally require dedicated phase tuning operation for individual elements, which is typically not supported for in-situ commercial mmWave radios, without special chip-set supports.

The default working mode of mmWave phased arrays is beam-steering in commercial systems, e.g. 60 GHz WiFi in the IEEE 802.11ad for short-range communication [27], 5G mmWave new radio (NR) [28], etc. Beam-steering is essential to align the transmitter (Tx) and receiver (Rx) beam, which is required in mmWave directional links. Typically, phased arrays employed at the Tx and Rx feature a set of pre-defined beams in a wide angular interval, and the best Tx-Rx beam pair can be selected via a brute-force search procedure. Beam-steering operation is enabled via setting phase shifts of all antenna elements simultaneously according to the beam-steering direction, which is supported in the default mode. However, other dedicated phase settings, e.g. to achieve a Hadamard matrix, might be not supported by the phased array under test. Therefore, it would be desirable that array calibration can be performed with phased array operating in beam-steering mode only. However, this has not been discussed in the literature, to the best knowledge of the authors.

In this paper, a novel array calibration method based on solving linear equations is proposed to measure the initial complex excitation coefficients of individual elements for the beam-steering uniform linear arrays (ULAs) that are widely used for various applications (e.g. LTE base station antennas, mmWave mobile handset antennas, etc.). The array complex signal is measured with a single probe antenna placed in the boresight while phase shifts of all elements are set according to beam-steering directions. It is found that the performance of the proposed method is mainly determined by the condition number of the beam-steering matrix. The factors that affect the beam-steering matrix condition, e.g. beam-steering interval, number of antenna elements, element spacing and number of steered beams, are investigated for ULAs. Furthermore, a strategy to select beam-steering directions, which offers lowest possible condition number for the ULA, is proposed. The proposed method is then numerically simulated and experimentally validated.

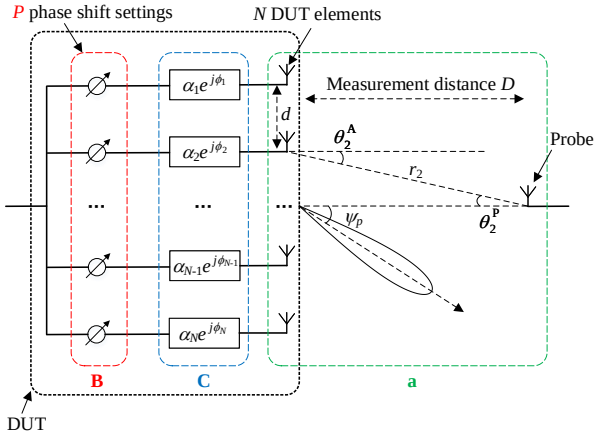

Figure 1. Beam-steering phase array calibration system schematic.

II. Method

A. Principle

The measurement system is illustrated in Fig. 1. Beam-steering operation is enabled by setting phase shifts by the phase shifters connected to the array elements according to the beam-steering direction of the array. The feed of the device under test (DUT) (which is enclosed by the dotted dark line in Fig. 1) is split into N branches, each connected to a phased shifter and an array element. The total number of phase shifter settings is P (with $P \geqslant N$, which is a condition for the proposed algorithm), allowing for beam-steering into P different directions. The initial complex excitation coefficient that needs to be determined in the n-th branch is denoted as $\alpha_n e^{j\phi_n}$, with α_n and ϕ_n denoting the initial amplitude and phase terms to be determined, respectively, for $n \in [1, N]$. The probe antenna is placed in the boresight direction of the DUT (with a measurement distance D) and aligned with the DUT's center. Our discussion is limited to a single-polarized ULA DUT, though its extension to the dual-polarized case is straightforward.

It is worth noting that the proposed calibration method in this paper is mainly discussed for the phased array architecture shown in Fig. 1, where the phase shifters are tuned according to beam steering angles for each antenna element. In many mmWave systems, the phased array antenna elements can

also be grouped into several subarrays, each of which is only connected to one phase shifter. In this case, each subarray is taken as an element in Fig. 1. The calibration is to compensate subarray-to-subarray inhomogeneities via tuning the phase shift according to beam steering angles for each subarray. However, calibrating the antenna elements within the subarray is not possible without the phase tuning per element. The proposed algorithm works as long as there is a phase shifter for each antenna or subarray, regardless of phase shift operation in the digital or analog domain. Therefore, the proposed method can be applicable to the digital and hybrid beamforming structure as well. In the proposed method, the phase tuning is performed in a digital manner for the digital beamforming structure. For the hybrid structure, the calibration might be required to compensate element-to-element inhomogeneities within each subarray independently or within the whole array. For one-by-one subarray calibration, the proposed algorithm can be directly applied only with the selected subarray activated. For the whole array calibration, the required phase shifts of individual elements can be generated via properly combining the phase shift operated in the analog domain and in the digital domain. Hence, the proposed calibration algorithm is a general method that is applicable for any beamforming structures.

According to Fig. 1, the signal model can be written as:

$$\mathbf{s} = \mathbf{B} \cdot \mathbf{C} \cdot \mathbf{a}, \tag{1}$$

where the matrices $\mathbf{B} \in \mathbb{C}^{P\times N}$ and $\mathbf{C} \in \mathbb{C}^{N\times N}$, and vector $\mathbf{a} \in \mathbb{C}^{N\times 1}$ characterize three distinct sub-parts of vector $\mathbf{s} \in \mathbb{C}^{P\times 1}$, respectively, as detailed below:

- Vector $\mathbf{s} = \{s_p\}$ is the complex S-parameter vector between the DUT antenna feed and probe antenna feed for P phase shifter settings, with its element s_p denoting the complex S-parameter for the p-th phase shifter setting. The complex vector $\boldsymbol{s}$ can be directly measured, e.g. via a vector network analyzer (VNA), in the setup.
- Matrix $\mathbf{B} = \{b_{pn}\}$, with its element b_{pn} denoting the complex excitation applied to the n-th DUT element for the p-th phase shifter setting. For a ULA shown in Fig. 1, b_{pn} can be expressed as:

$$\begin{aligned} b_{pn} &= \exp\big[-jk(n-1)d\sin(\psi_p)\big] \\ &= \Big[\exp\big(-jkd\sin(\psi_p)\big)\Big]^{n-1} \\ &= \big[\exp(-j2\pi f_p)\big]^{n-1}, \end{aligned} \tag{2}$$

  where k, d and ψ_p denote the wave number, ULA element spacing and beam-steering angle for the p-th phase shifter setting, respectively. $f_p = \frac{d\sin(\psi_p)}{\lambda}$ is the coefficient associated with ψ_p, which will be discussed later. λ is the wavelength. Beam-steering matrix $\mathbf{B}$ can be obtained using (2) with knowledge of the DUT antenna configuration, operating frequency and beam-steering direction settings, which is often available in phased array specifications. Note that no amplitude tapering is assumed for b_{pn} for simplicity. If amplitude tapering is applied, the tapering coefficient will be included in the calibration matrix $\mathbf{C}$. Therefore, the tapering coefficient can be compensated if known.
- Matrix $\mathbf{C} = \{c_n\}$ is the diagonal matrix to be determined, with its diagonal element $c_n = \alpha_n \exp(j\phi_n)$. In the ideal scenario, $\mathbf{C}$ is an identity matrix, indicating homogeneous RF chains connected to each DUT element. As explained, inhomogeneity exists among RF chains in practical phased array design, which needs to be calibrated out to ensure optimal phased array performance. The objective therefore is to determine the calibration matrix $\mathbf{C}$ based on knowledge of vector $\mathbf{s}$. The objective of the work is only to determine RF branch inhomogeneities via bulit-in beam-steering phase shifts, which is important in antenna system conformance and performance testing. In order to calibrate out the RF branch inhomogeneities, we still need to have the possibility to set the phase shifts separately for each RF branch. Note that the phased array is typically calibrated for a single carrier frequency. For a system with a wide bandwidth, we might have to divide the whole band into several small sub-bands and perform calibration in the center frequency of each sub-bands.
- Vector $\mathbf{a} = \{a_n\}$ is the coupling vector between the N DUT antenna element feeds and the probe antenna feed, with its element a_n denoting the coupling coefficient between the feed of the n-th element and the feed of the probe antenna. Assuming free space propagation scenario, we have

$$a_n = g_1(\theta_n^A) g_2(\theta_n^P) \frac{\lambda \exp(-jkr_n)}{4\pi r_n}, \tag{3}$$

  where $g_1(\theta_n^A)$ and $g_2(\theta_n^P)$ are complex antenna patterns for the n-th DUT antenna (in the direction of the probe antenna θ_n^A) and the probe antenna (in the direction of the n-th DUT antenna element θ_n^P), respectively. The fractional term expresses the free-space propagation coefficient. r_n is the distance between the probe antenna and n-th DUT antenna element. θ_2^A, θ_2^P, and r_2 are illustrated in Fig. 1, as an example. If the probe antenna is located in the near field of DUT array, the DUT antenna elements are in the different directions of the probe (i.e. $\theta_1^A \neq \theta_2^A \neq \cdots \neq \theta_N^A$ and $\theta_1^P \neq \theta_2^P \neq \cdots \neq \theta_N^P$). In the near field case, the unknown and non-negligible antenna gain difference among all elements in the different directions of the probe will be included in matrix $\mathbf{C}$, which would introduce deviations in the array calibration results. The proposed array calibration method in this paper works in the far field of the DUT array to avoid this problem, i.e. the DUT antenna elements are all in the same direction of the probe with $\theta_1^A = \theta_2^A = \cdots = \theta_N^A$ and $\theta_1^P = \theta_2^P = \cdots = \theta_N^P$. On the other hand, the proposed method like the other array calibration methods in the literature, works as well in principle when the probe antenna is located in other directions different from the boresight direction. However, the probe antenna is generally placed in the boresight direction in practice. By placing the probe antenna in the boresight direction of the phased array, the signal condition is good since the main beam of the element pattern is pointed towards

the boresight direction (i.e. reducing calibration error). Secondly, the phase response for each array element will be the same due to the fact that the impinging direction of the signal is perpendicular to the phased array (i.e. without knowledge of the DUT antenna array structure). Assuming the antenna pattern difference among all DUT elements negligible in the boresight direction, (3) can be simplified to an all-one vector.

From Eq. (1), the calibration matrix $\mathbf{C}$ can be determined by solving linear equations as below:

$$\boldsymbol{C} = \boldsymbol{B}^{+} \cdot \boldsymbol{s} \cdot \boldsymbol{a}^{+}, \tag{4}$$

where $()^{+}$ is the pseudo-inverse operator. In practical phased array system, phase shift operation in the phase shifters would introduce uncertainties in amplitude and phase, besides their quantization errors. Furthermore, it suffers from noise and nonidealities introduced by active components in the phased array (e.g. power amplifiers). Although the calibration matrix $\mathbf{C}$ can be solved using (4) in principle, its accuracy, however, is ruled by the condition number of matrix $\mathbf{B}$. The condition number of the matrix is an "amplification factor" that bounds the maximum relative change in the solution due to a given relative change in the noisy input data [25], [29]. To ensure good array calibration accuracy, matrix $\mathbf{B}$ with a small condition number is desirable.

B. Condition number of matrix $\mathbf{B}$

Beam-steering matrix $\mathbf{B}$ has the Vandermonde structure [29], with its complex node $z_p = \exp(j2\pi f_p)$ for $p \in [1, P]$. Many mathematical works have been reported in the literature on the condition numbers of Vandermonde matrices, see e.g. [29], [30]. Unfortunately, the Vandermonde matrix is typically ill-conditioned.

For a beam-steering phased array, depending on its application scenarios, its beam-steering capability is widely different in terms of beam-steering interval with respect to its nominal tilt direction. The interval depends on the array element radiation pattern (i.e. element pattern spatial filtering) and the array element spacing (i.e. grating lobe issue). For example, beam-steering intervals in the LTE base station are typically reported up to 15^o due to grating lobe effects introduced by large element spacing (e.g. 0.65 λ). For mmWave phased array employed in massive MIMO 5G base stations, the beam-steering interval can be up to 60^o in the azimuth plane and 30^o in the elevation plane, respectively. For mmWave mobile antenna handset antennas, full spherical coverage can be realized by employing multiple phased-arrays [31]. Wide-angle scanning with small gain fluctuation is a hot research topic for the mmWave phased array, see e.g. [31]. On the other hand, beam-steering step resolution can be rather small, since it is not very sensitive to phase shifter bits. Therefore, the number of beam-steering directions P can be set much larger than the number of DUT elements N in practice.

In principle, we can form a new matrix $\hat{\mathbf{B}} \in \mathbb{C}^{M \times N}$, which is generated by selecting M rows from P rows in matrix $\mathbf{B}$, with $N \leq M \leq P$. $\hat{\mathbf{B}}$ denotes the complex weights applied to the N DUT elements for the selected M phase shifter settings. Eq. (4) can be updated accordingly to obtain the calibration matrix $\mathbf{C}$, via replacing $\mathbf{B}$ by $\hat{\mathbf{B}}$. We have

$$\mathbf{C} = \hat{\mathbf{B}}^{+} \cdot \hat{\mathbf{s}} \cdot \mathbf{a}^{+}, \tag{5}$$

where $\hat{\mathbf{s}} \in \mathbb{C}^{M \times 1}$ is the corresponding S-parameter vector for the selected M phase shifter settings.

To ensure an optimal condition number of $\hat{\mathbf{B}}$, we can calculate the condition numbers of all possible $\hat{\mathbf{B}}$ for $\begin{pmatrix} M \\ P \end{pmatrix}$ total combinations, and select $\hat{\mathbf{B}}$ with the smallest condition number. However, there are several drawbacks of such brute-force search strategy. First, the computation complexity might be high, especially when P is large. Furthermore, it does not provide any insight into how condition number of $\hat{\mathbf{B}}$ is related to phased array beam-steering settings. The objective of our work is to achieve accurate array calibration for beam-steering phased array. Several practical aspects should be addressed:

- How does beam-steering interval and beam-steering resolution of the phased array affect the condition number of $\hat{\mathbf{B}}$?
- How does ULA phased array element spacing and number of elements affect the the condition number of $\hat{\mathbf{B}}$?
- How to set beam-steering directions (i.e. the number of beams and beam-steering angles) of the phased array to achieve the best algorithm performance?

Below, a novel strategy based on complex node distribution on the unit circle is described to determine the optimal $\hat{\mathbf{B}}$. Furthermore, the above-mentioned aspects are addressed in Section III based on the proposed method. Note that the proposed beam selection strategy in this paper is only applicable for the ULAs whose beam-steering matrix has the Vandermonde structure with its entry b_{pn} given by (2). For the uniform rectangular arrays (URAs) whose beam-steering matrixes are not Vandermonde, however, the proposed method cannot be directly applied.

C. $\hat{\mathbf{B}}$ *selection*

Let us denote the complex node vector $\mathbf{z} \in \mathbb{C}^{P \times 1}$ and the node angle coefficient vector $\mathbf{f}$, with its p-th element $z_p = \exp(j2\pi f_p)$ and $f_p = \frac{d \sin(\psi_p)}{\lambda}$ for $p \in [1, P]$, respectively. As explained, all complex nodes in the Vandermonde matrix $\mathbf{B}$ in (2) are distributed on the unit circle. Assume that we select M beam-steering directions from P directions, with beam-steering angle $\psi_1 < \psi_2 < ... < \psi_M$ with $\psi_m \in [-90^o, 90^o]$. As discussed below, the optimized M steering directions can be achieved with a uniform phase shift between two adjacent directions. The selected steering matrix

can thereby be expressed as:

$$\hat{\mathbf{B}} = \begin{bmatrix} 1 & e^{j\frac{2\pi d\sin(\psi_1)}{\lambda}} & \dots & e^{j\frac{2\pi d\sin(\psi_1)}{\lambda}(N-1)} \\ 1 & e^{j\frac{2\pi d\sin(\psi_2)}{\lambda}} & \dots & e^{j\frac{2\pi d\sin(\psi_2)}{\lambda}(N-1)} \\ \vdots & \vdots & \ddots & \vdots \\ 1 & e^{j\frac{2\pi d\sin(\psi_M)}{\lambda}} & \dots & e^{j\frac{2\pi d\sin(\psi_M)}{\lambda}(N-1)} \end{bmatrix} = \begin{bmatrix} 1 & e^{j(-\frac{M-1}{2}\sigma+\varepsilon)} & \dots & e^{j(-\frac{M-1}{2}\sigma+\varepsilon)(N-1)} \\ 1 & e^{j(-\frac{M-3}{2}\sigma+\varepsilon)} & \dots & e^{j(-\frac{M-3}{2}\sigma+\varepsilon)(N-1)} \\ \vdots & \vdots & \ddots & \vdots \\ 1 & e^{j(\frac{M-1}{2}\sigma+\varepsilon)} & \dots & e^{j(\frac{M-1}{2}\sigma+\varepsilon)(N-1)} \end{bmatrix}, \quad (6)$$

where σ represents the phase shift between the two adjacent steering directions and ε denotes the extra phase shift that one can freely set within a given range. Once σ and ε are selected, the steering matrix $\hat{\mathbf{B}}$ is determined and the steering angles can be calculated according to $\psi_m = \arcsin\{\frac{\lambda}{2\pi d}[(-\frac{M-1}{2} + m - 1)\sigma + \varepsilon]\}$. Note that the selected steering angles ψ_m will change with frequency if d and M are unchanged. As explained in Section II-A, however, this is typically not an issue in practice due to the small percent bandwidth at mmWave bands.

The determination of σ and ε is mainly ruled by the maximum separation between node angle coefficient (i.e. distance between f_M and f_1), which can be denoted as:

$$\delta = f_M - f_1, \quad (7)$$

with $f_m = \frac{d\sin(\psi_m)}{\lambda}$. As explained in [29], [30], a small condition number approaching 1 can be achieved for a Vandermonde matrix if its complex nodes $\hat{z}_m$ are uniformly distributed along a unit circle. Therefore, we propose a beam-steering selection method to achieve the optimal condition number of matrix $\hat{\mathbf{B}}$ in Eq. (5) as below:

1) With $\delta \geq 1$, the unit circle can be fully covered. Therefore, the complex nodes $\hat{z}_m$ can be uniformly distributed along the unit circle with any small interval between two adjacent nodes, implying that M can be any integer (no smaller than N). Under this condition, we can easily determine M steering angles ψ_m whose associated complex nodes are uniformly placed along the unit circle. That is, $\sigma = 2\pi/M$ and $\varepsilon \in (-\sigma/2, \sigma/2)$. The condition number of the steering matrix $\hat{\mathbf{B}}$ under such condition is equal to 1, implying robust and accurate array calibration performance. However, this condition requires a full-range beam-steering angle interval (i.e. $[-90^o, 90^o]$) and phased array element spacing $d \geq \lambda/2$.
2) With $\delta < 1$, the unit circle is only partially covered, as shown in the black curve covered part in Fig. 2 (a) and (b) (parameter setting of the ULA explained in Section III). Under this condition, the beam-steering selection strategy is proposed as below. The M complex nodes can still distribute uniformly on the unit circle if M satisfies the boundary below:

$$M \leq 1/(1-\delta). \quad (8)$$

For a M within the above boundary, we can still select M beam-steering angles ψ_m to ensure the complex nodes having uniform spacing. However, the selection is not as flexible as in condition 1). Instead, we have to make sure the complex nodes are uniformly distributed along the unit circle within the given range $[2\pi f_1, 2\pi f_M]$, as illustrated in Fig. 2 (a). This figure demonstrates that the complex nodes are uniformly located along the unit circle when the condition in (8) is satisfied. In this case, $\sigma = 2\pi/M$ and $\varepsilon \in (-\varepsilon_{max}/2, \varepsilon_{max}/2)$, where $\varepsilon_{max} = 2\pi(f_m - f_1 - 1) + \sigma$ and $\varepsilon_{max} < \sigma$. In this way, the composed steering matrix $\hat{\mathbf{B}}$ is also well-conditioned.
3) If the condition in Eq (8) is not met, M selected complex nodes can not be uniformly placed on the unit circle, as illustrated in Fig. 2 (b). For the same unit circle coverage (i.e. beam-steering angle interval) as in (a), the complex nodes cannot uniformly distributed on the unit circle when M is beyond the boundary defined in (8). In this case, we select the beam-steering angles ψ_m to have the complex nodes uniformly distributed within $[2\pi f_1, 2\pi f_M]$. That is, $\sigma = \frac{2\pi(f_M - f_1)}{M-1}$ and $\varepsilon = 0$. The condition number of the steering matrix $\hat{\mathbf{B}}$ will be larger than 1, leading to unreliable and less accurate calibration results.

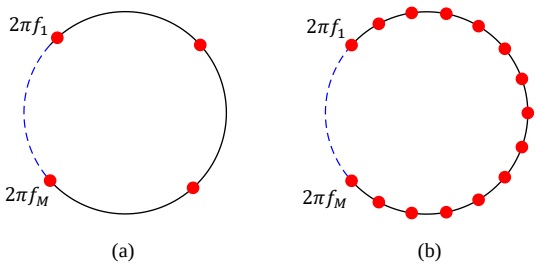

Figure 2. An illustration of the complex node distribution for M within the boundary condition with $M = 4$ (a) and beyond the boundary condition with $M = 15$ (b). The half range steering angle is $\Phi_P = 50^o$ with $\bar{\Phi}_P = 48.6^o$.

According to the above discussion, we can conclude that the full coverage of the unit circle can be achieved with $\delta \geq 1$ or $\frac{M-1}{M} \leq \delta < 1$. Therefore, the minimum beam-steering range to ensure the full circle coverage is given by

$$\bar{\Phi}_P = \arcsin(\frac{M-1}{M} \cdot \frac{\lambda}{2d}). \quad (9)$$

III. Numerical Simulation

A ULA composed of four array element with 0.5λ element spacing is used in the numerical simulation (to mimic the ULA employed in the measurement as detailed later) unless otherwise stated. Below we investigate how the bit number of phase shifters, beam-steering interval, ULA parameters would affect the condition number of $\hat{\mathbf{B}}$.

A. Bit number of phase shifters

As discussed, we should select beam-steering ψ_m such that f_m is uniformly distributed on the covered circle for $m \in [1, M]$. Note that the distribution will not be uniform if the beam-steering angles have constant step, due to the sin function relationshop between ψ_m and f_m. To implement the

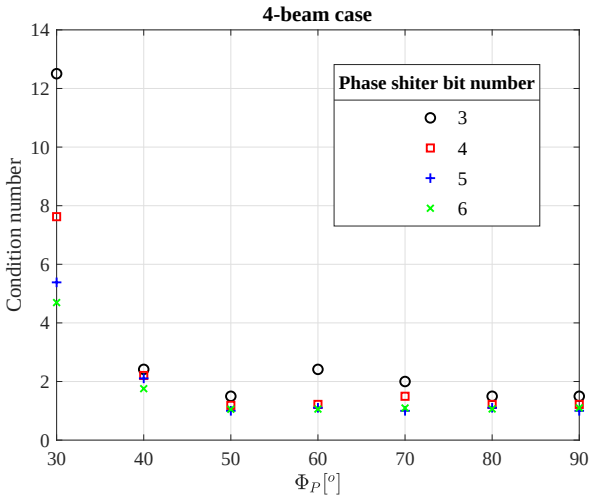

Figure 3. The impact of phase shifter bit-number on condition number for different Φ_P settings ($M = N = 4$).

selected steering matrix $\hat{\mathbf{B}}$, phase shifters should be used. For digital phase shifters, the phase adjust resolution is determined by the phase shifter bit number, with phase range 360^o typically supported. Assuming that we use the phase shifters with a bit number of K, i.e. with a phase shift step-size $\Delta = \frac{2\pi}{2^K}$, to implement the matrix $\hat{\mathbf{B}}$ in (6), the phase shift errors will be bounded to $[-\Delta/2, \Delta/2]$ (assume phase shifter uncertainty is negligible). For instance, given $N = 4$, $M = 5$, $\sigma = \frac{360^o}{M} = 72^o$ and $\varepsilon = 5^o$, the round-off phase errors of matrix $\hat{\mathbf{B}}$ in (6) by using the 2-bit phase shifters and the 3-bit phase shifters are $\begin{bmatrix} 0^o & -41^o & 8^o & -33^o \\ 0^o & -23^o & 44^o & 21^o \\ 0^o & -5^o & -10^o & -15^o \\ 0^o & 13^o & 26^o & 39^o \\ 0^o & 31^o & -28^o & 3^o \end{bmatrix}$ and $\begin{bmatrix} 0^o & 4^o & 8^o & 12^o \\ 0^o & 22^o & -1^o & 21^o \\ 0^o & -5^o & -10^o & -15^o \\ 0^o & 13^o & -19^o & -6^o \\ 0^o & -14^o & 17^o & 3^o \end{bmatrix}$, respectively. Both of them are within $[-\Delta/2, \Delta/2]$ as expected. In general, to implement a given matrix matrix $\hat{\mathbf{B}}$, the phase shifters with a smaller bit-number will introduce larger round-off phase errors, resulting in a stronger impact on the condition number of $\hat{\mathbf{B}}$. Furthermore, the phase shifters with a bit number K_1 might well implement matrix $\hat{\mathbf{B}}$, i.e., without introducing any round-off errors, which implies that any phase shifters with a bit number $K \geq K_1$ can well implement the matrix $\hat{\mathbf{B}}$ as well. In this case, the phased shifters have negligible impact on the condition number of the matrix $\hat{\mathbf{B}}$, as long as the bit number satisfying $K \geq K_1$.

The impact of the bit-number of a phase shifter is illustrated in Fig. 3 for 4-beam cases (i.e. $M = N = 4$). We can see that a smaller condition number can be achieved with a higher-bit phase shifter as expected, due to more accurate phases can be generated. The bit-number affects the condition number only when the beam-steering interval is small. With bit-number larger than 4, the impact of bit-number on condition number is negligible. In the simulation results below, the phase shifter bit is set to 6, i.e., with LSB 5.625^o, to mimic settings for the AiP employed in the measurement.

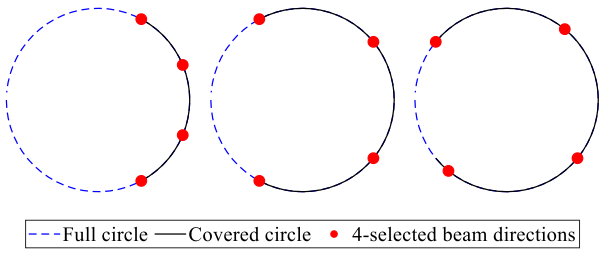

Figure 4. The four selected complex nodes on the unit circle for $\Phi_P = 20^o$ (left), 40^o (middle) and 50^o (right) ($M = N = 4$).

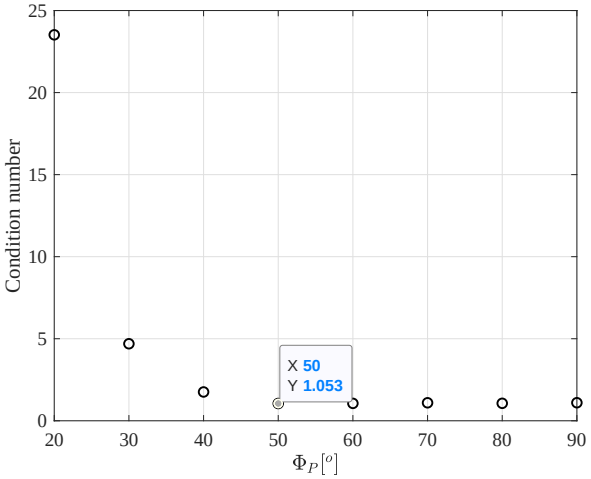

Figure 5. Condition number of matrix $\hat{\boldsymbol{B}}$ for different Φ_P settings ($M = N = 4$).

B. Beam-steering interval

As stated in Section II-C, we can ensure that the selected M complex nodes can be uniformly distributed on the full circle (thereby leading to a small condition number), when we have half range steering interval $\Phi_P \geq \bar{\Phi}_P$. For the four-element ULA with 0.5λ element spacing, we have $\bar{\Phi}_P = 48.6^o$ using Eq. (9). Following the complex node selection in Section II-C, the selected four selected complex nodes are shown in Fig. 4 for $\Phi_P = 20^o$, 40^o and 50^o, respectively. The complex nodes, though uniformly distributed, can only cover part of the circle with $\Phi_P < \bar{\Phi}_P$, while a full circle can be covered with uniformly distributed complex nodes with $\Phi_P \geq \bar{\Phi}_P$. The condition number of $\hat{\mathbf{B}}$ is shown in Fig. 5 for different steering angle interval Φ_P. A condition number approaching 1 can be achieved with $\Phi_P \geq \bar{\Phi}_P$, as expected. The condition number converges to 1 when complex nodes can be uniformly distributed on the unit circle. Therefore, we can conclude that the condition number is mainly ruled by the phased array steering angle interval.

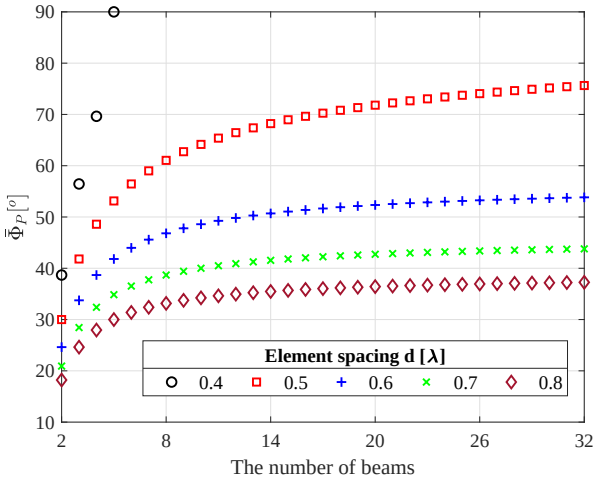

Figure 6. The impact of number of beams and element spacing on the required beam-steering interval threshold.

C. ULA parameters

1) Number of elements: From Eq. (9), we can also conclude that a larger beam-steering interval threshold $\bar{\Phi}_P$ would be required if the number of array elements N increases. For example,we have $\bar{\Phi}_P = 30^o$, 48.6^o, 61.0^o and 69.6^o for half-wavelength ULA with $N = 2$, 4, 8, and 16 elements, respectively.

2) Element spacing: According to Eq. (9), a larger element spacing would lead to a smaller beam-steering interval threshold $\bar{\Phi}_P$, which can be clearly observed in Fig. 6.

3) Number of beam-steering directions: The impact of M on the condition number is shown in Fig. 2 and Fig. 6. We can conclude that for a ULA with a given element spacing, the beam-steering interval threshold goes up as the number of beams increases. Therefore $M = N$ can render smallest possible condition number and also minimum number of measurements. Note that in practical measurement, a large M setting might be beneficial due to statistical averaging effect.

IV. Measurement Validations

A. Measurement system

A 4×4 mmWave phased array AiP operating from 26.5 GHz to 29.5 GHz was utilized in the experimental campaign. The AiP integrates four AWMF-0158 chips with 16 single-polarized patch antennas [32]. The patch element spacing is 5.45 mm (i.e. roughly 0.5 λ at 28 GHz). Each AiP element is connected to a 5-bit programmable attenuator (with LSB 0.5 dB) and a 6-bit programmable phase shifter (with LSB 5.625^o). Individual amplitude and phase control of each phased array AiP element is automated, with help of the control computer, which can significantly facilitate the measurement effort and time.

The measurement setup diagram is illustrated in Fig. 7 and a measurement photo is shown in Fig. 8, which is composed of the 4×4 mmWave phased array AiP, the probe antenna (standard gain horn antenna Flann 22240-20), a vector network analyzer (VNA), a DC power supply for the AiP and a

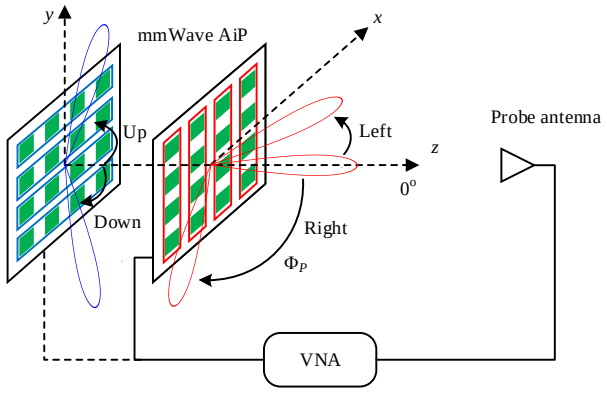

Figure 7. Diagram of the measurement setup.

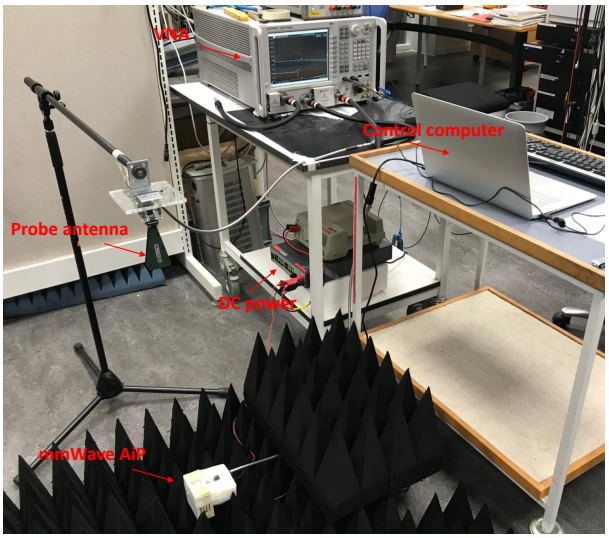

Figure 8. A photo of the measurement system.

control computer for automating the measurement campaign and storing the measured data. The probe antenna was placed to the boresight of the AiP, with aligned polarization. The distance between the AiP and probe antenna was around 0.7 m, which is larger than the far field distance of the AiP (around 0.1 m) at 28 GHz. The S-parameters between the mmWave AiP antenna feed and the probe antenna feed were recorded at 28 GHz for each complex excitation setting for the AiP, with AiP operating in receive (Rx) mode. As discussed, the developed mmWave phased AiP experimental platform offers complex excitation coefficient control of individual AiP elements, thereby enabling both the REV method measurement and the conventional beam-steering operation in an automated manner [32].

B. Calibration Measurement

To evaluate how accurate our proposed array calibration method works in practice, a reference calibration method is required to obtain the actual initial excitation of the AiP elements (i.e. the "ground truth"). As discussed, array calibration with "on-off" method with the help of a near-field scanner is dominantly used in the industry. However, such method re-

quires highly accurate repositioning of the probe antenna, high isolation between DUT elements, and precise knowledge of the DUT element configuration. These requirements, however, are typically difficult to be met for practical mmWave AiP systems. For example, the mmWave AiP in our measurement is a "black-box" design with its patch antenna array covered. Furthermore, the isolation among AiP elements is less than -15 dB according to manufacture specification. Therefore, it is desirable to employ the "all-on" calibration method. In the all-on calibration mode, it does not require knowledge of the DUT antenna configuration, and it can include mutual coupling effect in the calibration as in normal operation mode of the phased array. In this paper, the well-known REV calibration is adopted as the reference method.

1) REV calibration measurement: The REV calibration method is an amplitude-only measurement method, which is desirable especially when accurate phase measurement is difficult. In the REV measurement, the complex S-parameters of the AiP array are recorded in the VNA when phase of one AiP element is rotated from 0^o to 360^o, with phase excitation for the other AiP elements unchanged at 0^o. This process is repeated for all the AiP elements sequentially. Note that the amplitude excitation of all AiP elements are set to the same attenuation in the REV procedure. Only the amplitudes of the S-parameter measurements are used in the REV method, though phase measurements are available. In our measurements, a total of 16 (number of AiP elements) $\times$ (2^6+1) (number of phase rotations per element) measurements were performed. We can obtain the calibration matrix $\mathbf{C}$ for all 16 AiP elements applying the REV algorithm.

2) Beam-steering calibration measurement: The proposed method is a complex signal measurement method, which requires both amplitude and phase measurement. In the beam-forming measurement, the complex S-parameters are recorded in the VNA when the phase excitation coefficients for all AiP elements are set according to the beam-steering directions. Beam-steering operations on two axes were performed, as illustrated in Fig. 7, i.e. over the x axis (denoted as horizontal beam-steering) and over the y axis (denoted as vertical beam-steering). To exploit the mmWave AiP beam-steering full capability, the linearly progressing phase shift between elements was tuned from 0^o to 360^o with the LSB 5.625^o (i.e. a total of 65 steps), which corresponds to a steering angle $\psi_p \in [-79.2^o, 79.2^o]$ with a total of 65 steering directions. The steering angles, which are set according to uniform phase tuning step, are therefore non-uniformly distributed within the steering angle interval. Note that only four complex signal measurements (corresponding to four beam-steering directions) are needed in principle according to (5) to calibrate the phased array. Note that the proposed complex-signal method only requires N complex signal measurements, which is the minimum number of required measurements in the literature. In [25], [26], it was demonstrated that $N+1$ complex signal measurements would be needed even with individual phase control of array elements. For amplitude-only measurements, many more measurements are required [14].

In typical beam-steering operation, only relative phase relationship is important to ensure beam-steering power pattern, while absolute phase setting of array elements for different beams is not required. In our measurement, we need to obtain both array amplitude and phase measurement for different beam-steering angles. Therefore, the phases of AiP elements are normalized to the first ULA element for different beams to ensure consistent array phase measurement for different beam-steering directions.

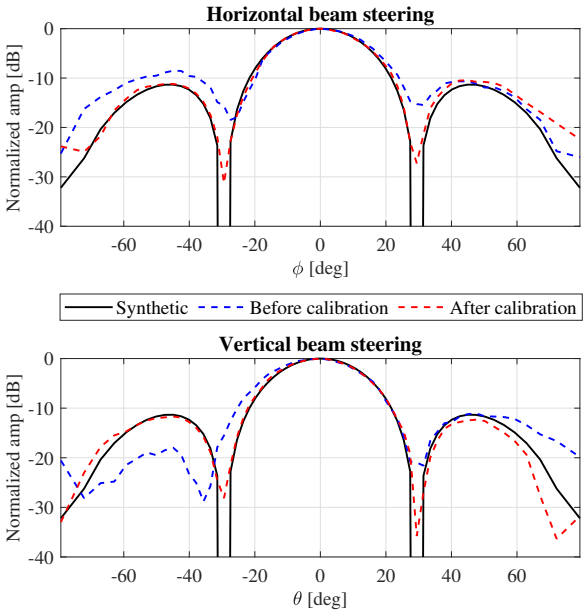

Figure 9. Comparison of measured AiP beam patterns before and after calibration with the ideal synthetic pattern (i.e. with uniform initial excitations) for both horizontal and vertical beam-steering measurements.

Based on our proposed method, the initial excitation coefficients between the 1×4 ULA elements can be determined. Each ULA element is enclosed in red and it is a sub-array composed of 4×1 patch elements based on horizontal beam-steering measurements. Similarly, we can obtain the initial excitation coefficients between the 4×1 ULA elements based on the vertical beam-steering measurements, where each element is enclosed in blue and is composed of 1×4 patch elements.

3) Validation of AiP calibration algorithm: To examine the effectiveness of array calibration for the AiP, beam-steering measurements of the uncalibrated AiP and calibrated AiP were performed. For the uncalibrated case, the default mode of the AiP is utilized (i.e. with 0 dB attenuation and 0^o phase shift set in the attenuator and phase shifter of AiP, respectively, for all elements). As explained, inhomogeneities exist among RF chains in the uncalibrated AiP, though the same excitation coefficients were set. For the calibrated case, the REV method was applied to detect inhomogeneities in the uncalibrated AiP first and the element-to-element inhomogeneities were then compensated via setting the compensated phase and amplitude excitation coefficient for each AiP element. As shown in Fig. 9, the uncalibrated and calibrated AiP beam patterns are compared with the ideal synthetic pattern where the initial excitations of the array elements are set to 1 for both horizontal and vertical beam-steering measurements. The patterns are

normalized to the boresight direction. Although the main beam pointing angle is not changed before and after calibration, the measured beam pattern after calibration matches better with the synthetic pattern than the measured pattern before calibration, in terms of the shape of the main beam, the locations and depth of the nulls, and the shape and level of the sidelobes. As a comparison, null depths can be significantly improved by the AiP calibration, where a null depth of 30 dB can be achieved. Furthermore, more symmetric pattern can be achieved after the AiP calibration. These observations indicate that the AiP calibration indeed improves the beam pattern, as expected in [32]. It can be found from the bottom of Fig. 9 that the uncalibrated pattern has a wider main beam and lower side lobes than the calibrated pattern and the synthetic pattern for the vertical beam-steering. This might due to the amplitude tapering effect in the uncalibrated array, which can be seen from the obtained excitation coefficients later. The tapering effect will decrease the directivity of the phased array. The wider main beam and lower side lobes imply that the amplitude excitation coefficients of the individual antenna elements are nonuniform. Thus, the calibration procedure should be performed.

Note that a well-designed phased array might not need any calibration, e.g. in [33] where a scalable 32-element phased array based on a 2×2 unit cell is built. Symmetrically locating the 2×2 unit cells, the built 32-element phased array can achieve the array pattern with its main beam width close to the theoretical value and the sidelobe level lower than -12 dB without calibration. Basically, most commercial mmWave 5G arrays rely on the tight manufacturing tolerance of integrated circuits to avoid the requirement of calibration, if we only focus on the main beam pointing angle and the sidelobe level (e.g. the phased arrays on the user equipment side) since they are not very sensitive to array element excitations. However, for applications like base station antenna arrays, the locations and depth of the nulls should be also considered, e.g. a 30-dB stringent requirement on null depth, which requires performing the phased array calibration to reduce the gain and phase difference between the elements.

C. Measurement results

1) ULA reconstruction in the REV measurement: As explained, we can only obtain four initial excitation coefficients for the 1×4 ULA elements in the horizontal beam-steering measurements, and four for the 4×1 ULA elements in the vertical beam-steering measurements. As a comparison, 16 initial excitation coefficients of all phased array elements can be obtained in the REV measurements. Therefore, to be able to evaluate the array calibration results achieved with the proposed method, we need to reconstruct the same 1×4 ULA and 4×1 ULA from the 4×4 phased array for the REV method. As illustrated in Fig. 7, a 1×4 ULA can be reconstructed based on the 4×4 phased array once the initial excitation coefficients for 16 elements are detected with the REV method. We can sum up complex initial excitation coefficients of AiP elements on the same column directly to form a 1×4 ULA on the x axis, with the known initial

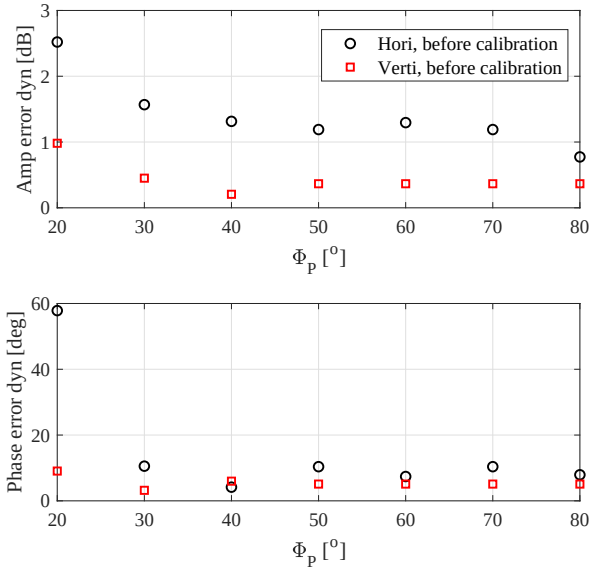

Figure 10. The amplitude and phase errors for different steering angle intervals in the measurement.

excitation coefficients in the REV method. Similar operations can be performed to form a 4×1 ULA on the y axis, by summing up complex initial excitation coefficients on the same row. After the reconstruction, we can compare the complex initial excitation coefficients of the reconstructed ULAs in the REV measurement and in the beam-steering measurements. Note that for the calibrated AiP case, complex initial excitation coefficients of the reconstructed ULAs in the REV measurement are compensated, and therefore we have the same excitation coefficient for all AiP elements in principle. However, the excitation coefficients for the calibrated AiP might still slightly differ in practice due to uncertainties in the AiP. This can be seen in Fig. 9 as well, where we have ideal symmetric pattern in the synthesis yet only approximately symmetric pattern in the measurement for the calibrated AiP.

2) mmWave AiP beam-steering setting: To investigate the impact of beam-steering angle interval on the array calibration accuracy, Φ_P can be set to a value based on the available beam-steering measurements. The results are shown in Fig. 10 for the horizontal and vertical beam-steering measurements for the uncalibrated AiP as an example. The associated condition numbers of $\hat{\mathbf{B}}$ for the four-element ULA for different steering intervals are shown in Fig. 5. The amplitude and phase error are the deviation of the estimated initial complex excitation coefficients between the REV method and proposed method. The four beam-steering directions in $\hat{\mathbf{B}}$ are selected according to the proposal in Section II-C. As discussed, when $\Phi_P < \bar{\Phi}_P$ is set, the array calibration accuracy will suffer due to large condition number of $\hat{\mathbf{B}}$. For example, an amplitude peak-to-peak error and a phase peak-to-peak error of up to 2.5 dB and 60^o for the horizontal beam-steering measurements, and up to 1 dB and 10^o for the vertical beam-steering measurements can be seen, respectively, with $\Phi_P = 20^o$. Although the condition number is the same for horizontal and vertical beam-steering measurements, the measured array calibration accuracy is

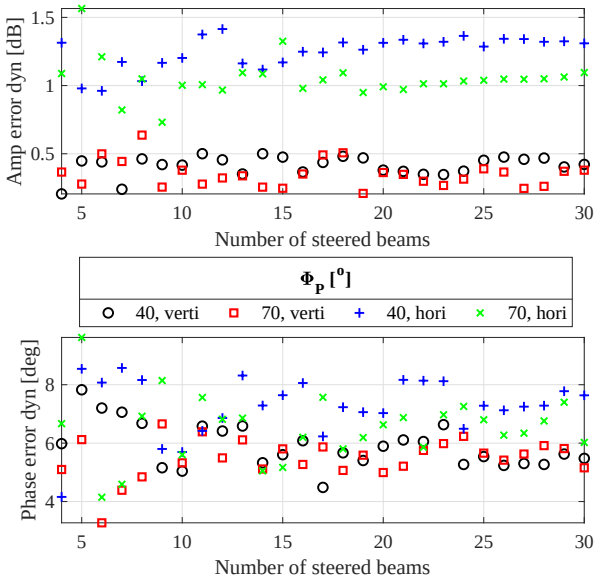

Figure 11. The amplitude and phase errors for different number of steering angles in the measurement.

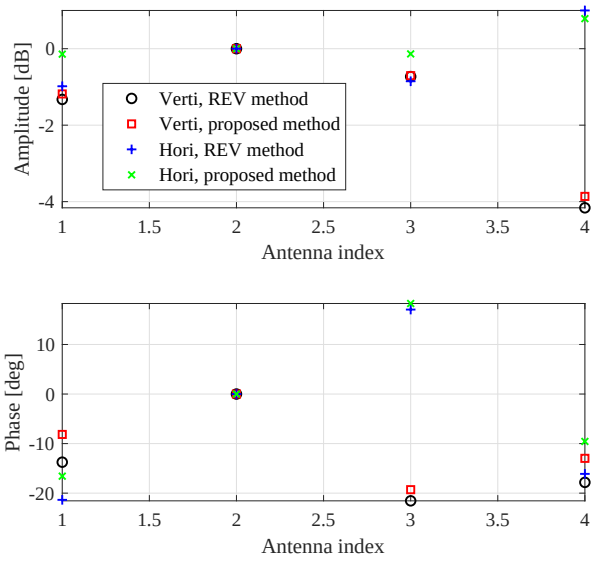

Figure 12. Measured excitation coefficients for the AiP elements in the uncalibrated AiP. The amplitude and phase coefficients are normalized to ULA element 2.

different. This might be due to the fact that horizontal beam-steering operation is more noisy and presents high uncertainty in the mmWave AiP. When $\Phi_P \geq \bar{\Phi}_P$ ($\bar{\Phi}_P = 48.6^o$) is set, much smaller array calibration errors can be observed, as expected. Note that it might not be beneficial to set a large Φ_P in practical measurements. The phase measurement of the mmWave AiP might be inaccurate when the phased array beam is steered too far away from the probe antenna direction, due to low SNR when array power is significantly attenuated.

Besides the beam-steering interval, another parameter to be set for the mmWave phased array AiP is the number of beam-steering directions. In the measurement results shown in the Fig. 11, we observe that the array calibration accuracy tends not to depend on the number of beams. This might be due to the fact that we can average out the measurement uncertainties when the number of beams is large from the statistical point of view. Worse array calibration accuracy is observed in the horizontal beam-steering measurements, compared to that in the vertical beam-steering measurements, which is consistent with observation in Fig. 10. We use all the 65 beam-steering directions with $\Phi_P = 79.2^o$ in the analysis below for simplicity. Note that we often use as few measurements as possible in practice to reduce the measurement time.

3) Array calibration accuracy:

a) Initial complex excitation coefficients: The initial complex excitation coefficients obtained with the REV method and the proposed method are shown in Fig. 12 for the 1×4 ULA (i.e. horizontal beam-steering on the x axis direction) and 4×1 ULA (i.e. vertical beam-steering on the y axis direction) for the uncalibrated AiP as an example. The amplitude and phase excitation difference among elements can vary up to 5 dB and 40^o, respectively, indicating that RF chains are not equal in the uncalibrated AiP. Note that the excitation amplitude tapering effect can be observed in the uncalibrated array for the vertical beam-steering, i.e. the

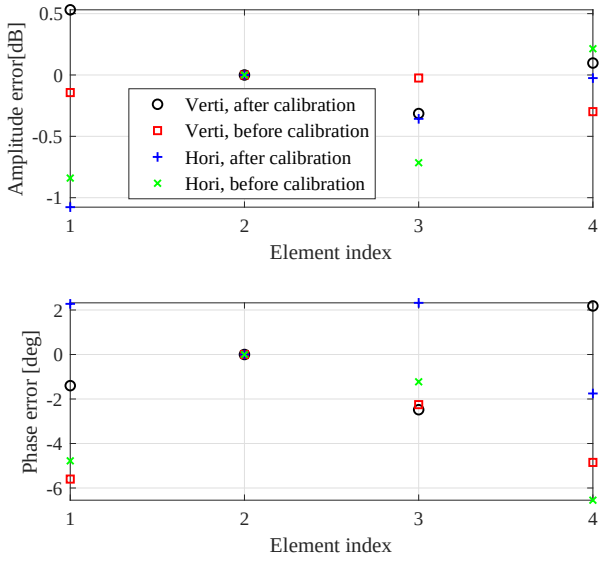

Figure 13. Measured excitation coefficient estimation accuracy for the AiP elements. The amplitude and phase coefficients are normalized to ULA element 2.

amplitude excitation values of the elements located around the array center (elements 2 and 3) are larger than the amplitude excitation values of the elements located around the array edge (elements 1 and 4), which explains the uncalibrated pattern in Section IV-B3. The measured phase terms are normalized to the second ULA element for comparison purpose. This is due to the fact that the phase terms estimated in the REV method are relative to the composite complex field, which is typically unknown. Therefore, only relative phase between ULA elements can be detected. For the proposed method, we can measure the absolute phase since it is based on complex

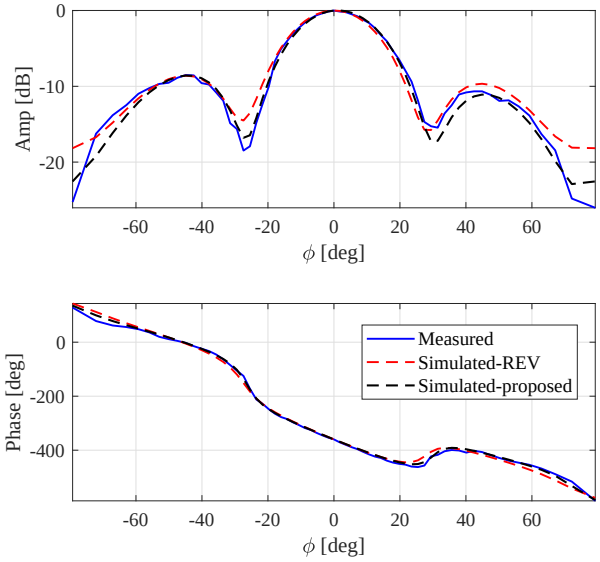

Figure 14. Measured and simulated beam-steering array power (top) and phase (below) in the horizontal beam-steering measurements for the uncalibrated AiP.

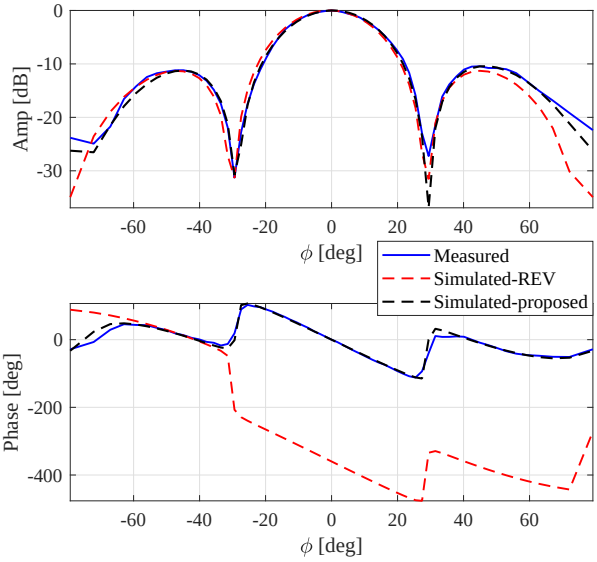

Figure 15. Measured and simulated beam-steering array power (top) and phase (below) in the horizontal beam-steering measurements for the calibrated AiP (with the REV method).

signal measurements. Note that absolute phase measurement is required when accurate distance is required, e.g. for the radar applications.

The initial complex excitation coefficients estimated with the proposed method match well with those achieved by the REV method for all cases, as shown in Fig. 13. The amplitude and phase errors of the calibration results achieved with the two methods are shown in Fig. 13 for the uncalibrated and calibrated AiP. The amplitude and phase deviation within ± 0.5 dB and $\pm 5^o$ can be observed, respectively. The small deviation demonstrates the calibration accuracy of the proposed method is comparable to the REV method, which validates the feasibility and effectiveness of the proposed method. The deviations might be introduced by the mmWave AiP amplitude and phase control uncertainty. Furthermore, component characteristics might drift over time as well, since the two measurements were performed over 2 hours. As discussed, we should expect 0 dB and 0^o for all ULA elements for the calibrated AiP cases for ideal AiP. However, the AiP suffers from uncertainties in practical setups.

b) Simulated and measured beam-steering array pattern: Based on initial excitation coefficients estimated with the REV method and the proposed method and the known mmWave AiP antenna configuration, we can reconstruct the power and phase array pattern for the beam-steering measurements. The measured and simulated phased array AiP power and phase patterns are shown in Fig. 14, Fig. 15, Fig. 16 and Fig. 17 for the uncalibrated AiP horizontal beam-steering measurement, calibrated AiP horizontal beam-steering measurement, uncalibrated AiP vertical beam-steering measurement and calibrated AiP vertical beam-steering measurement, respectively. As we can see, when there exists a null in the amplitude pattern, a 180^o phase reversal would appear, causing discontinuity in the array phase pattern, as expected. Note that isotropic elements

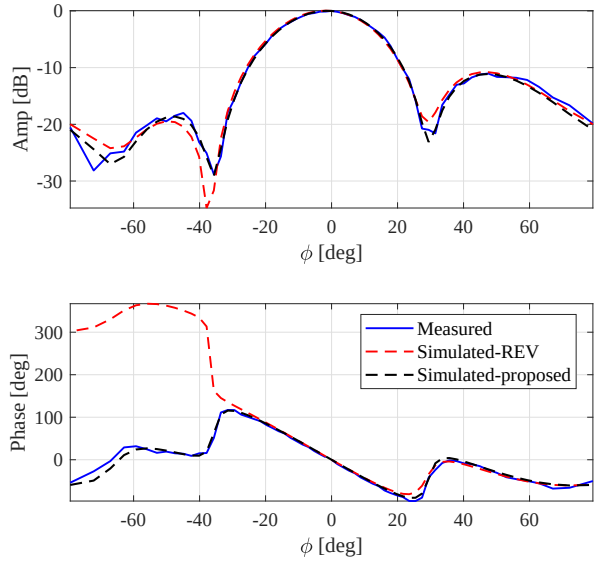

Figure 16. Measured and simulated beam-steering array power (top) and phase (below) in the vertical beam-steering measurements for the uncalibrated AiP.

patterns are assumed in the simulation since patch element patterns are unknown.

Generally speaking, a good agreement can be achieved between simulated patterns (both with the REV method and the proposed method) and measured patterns, where main beams, side lobes and null directions can be well reproduced. Small deviations exist in the pattern, e.g. in the null depth and when the beam-steering directions $|\Phi_p|$ are larger than 60^o. The null depth is highly sensitive to array calibration accuracy. The proposed method offers good agreement with measured data even for the null depth, which indicates high accuracy of

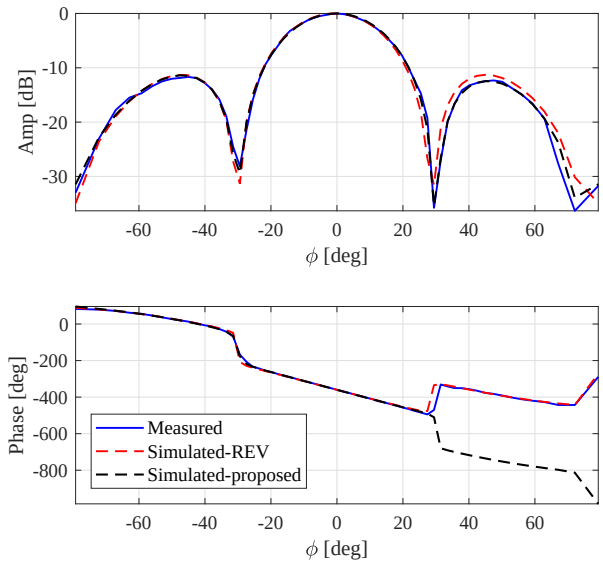

Figure 17. Measured and simulated beam-steering array power (top) and phase (below) in the vertical beam-steering measurements for the calibrated AiP (with the REV method).

the proposed method. The deviation in the power and phase patterns where beam-steering directions are large is mainly introduced by the assumption of isotropic element radiation pattern. Although the patch antenna pattern in the mmWave AiP has wide beam-width, its gain pattern is greatly attenuated for large beam-steering directions. Note that the simulated array power pattern with the REV method is symmetric for the calibrated AiP due to the fact that the complex excitation coefficients of array elements are compensated, as explained.

V. Conclusion and Future Work

In this paper, a novel array calibration method based on solving linear equations is proposed to measure the initial complex excitation coefficients of the individual elements for the phased arrays only supporting beam-steering mode. The proposed method works for phased array operating in default beam-steering mode and only requires minimum number of measurements (i.e. the same as the number of the phased array elements), compared to the state-of-art methods. The performance of the proposed method is mainly determined by the condition number of the beam-steering matrix, which is found to be Vandermonde-structured for the ULA. To render a small condition number for the beam-steering matrix, it is proposed to select the beam-steering directions where the associated complex nodes are uniformly distributed on the unit circle. The factors that affect the beam-steering matrix condition, e.g. beam-steering angle interval and resolution angle, number of antenna elements and element spacing and number of steered beams, are investigated for a ULA. It is found that the condition number is mainly determined by the beam-steering intervals, although other factors (i.e. AiP element number and AiP element spacing) can affect the condition number as well.

The proposed method is experimentally validated in a mmWave phased array AiP at 28 GHz via comparing results with the well-known REV calibration method. The initial complex excitation coefficients estimated with the proposed method match well with those achieved by the REV method for both the calibrated AiP and uncalibrated AiP, with the amplitude and phase errors within ± 0.5 dB and $\pm 5^o$, respectively. A good agreement can be achieved between simulated patterns (both with the REV method and the proposed method) and measured patterns, where main beams, side lobes and null directions can be well reproduced.

There are several logical extensions of the proposed method in the future. The discussion is limited to ULAs in the paper, and it is of interest to understand how we can extend it for arbitrary array configuration. Further, the proposed method requires complex signal measurement, which might be challenging for mmWave systems due to lack of antenna connectors and inaccurate measurement of phase. Therefore, it would be desirable that array calibration can be realized for beam-steering mode phased array with amplitude-only measurement. Furthermore, it is demonstrated the algorithm would fail when beam-steering matrix is ill-conditioned (especially when the beam-steering interval is small), which necessitates strategies to reduce the condition number for such phase arrays.

References

[1] T. S. Rappaport, R. W. Heath Jr, R. C. Daniels, and J. N. Murdock, *Millimeter wave wireless communications*. Pearson Education, 2015.

[2] R. He, B. Ai, G. Wang, Z. Zhong, C. Schneider, D. A. Dupleich, R. S. Thomae, M. Boban, J. Luo, and Y. Zhang, "Propagation channels of 5g millimeter-wave vehicle-to-vehicle communications: recent advances and future challenges," *IEEE Veh. Technol. Mag.*, vol. 15, no. 1, pp. 16–26, 2019.

[3] R. He, B. Ai, G. L. Stüber, G. Wang, and Z. Zhong, "Geometrical-based modeling for millimeter-wave mimo mobile-to-mobile channels," *IEEE Trans. Veh. Technol.*, vol. 67, no. 4, pp. 2848–2863, 2017.

[4] K. Guan, B. Peng, D. He, J. M. Eckhardt, S. Rey, B. Ai, Z. Zhong, and T. Kürner, "Channel characterization for intra-wagon communication at 60 and 300 ghz bands," *IEEE Trans. Veh. Technol.*, vol. 68, no. 6, pp. 5193–5207, 2019.

[5] K. Guan, G. Li, T. Kürner, A. F. Molisch, B. Peng, R. He, B. Hui, J. Kim, and Z. Zhong, "On millimeter wave and thz mobile radio channel for smart rail mobility," *IEEE Trans. Veh. Technol.*, vol. 66, no. 7, pp. 5658–5674, 2016.

[6] S. Geng, J. Kivinen, X. Zhao, and P. Vainikainen, "Millimeter-wave propagation channel characterization for short-range wireless communications," *IEEE Trans. Veh. Technol.*, vol. 58, no. 1, pp. 3–13, 2008.

[7] Y. Zhang and J. Mao, "An overview of the development of antenna-in-package technology for highly integrated wireless devices," *Proc. IEEE*, vol. 107, no. 11, pp. 2265–2280, 2019.

[8] W. Roh, J.-Y. Seol, J. Park, B. Lee, J. Lee, Y. Kim, J. Cho, K. Cheun, and F. Aryanfar, "Millimeter-wave beamforming as an enabling technology for 5g cellular communications: Theoretical feasibility and prototype results," *IEEE Commun. Mag.*, vol. 52, no. 2, pp. 106–113, 2014.

[9] R. C. Hansen, *Phased array antennas*. John Wiley & Sons, 2009, vol. 213.

[10] F. Scattone, D. Sekuljica, A. Giacomini, F. Saccardi, A. Scannavini, L. Foged, E. Kaverine, N. Gross, and P. Iversen, "Comparative testing of devices in a spherical near field system and plane wave generator," in *2019 Antenna Measurement Techniques Association Symposium (AMTA)*. IEEE, 2019, pp. 1–3.

[11] R. J. Weber and Y. Huang, "An automatic calibration system for smart antenna arrays," in *2009 IEEE Antennas and Propagation Society International Symposium*. IEEE, 2009, pp. 1–4.

[12] L. Kuai, J. Chen, Z. H. Jiang, C. Yu, C. Guo, Y. Yu, H.-X. Zhou, and W. Hong, "A n260 band 64 channel millimeter wave full-digital multi-beam array for 5g massive mimo applications," *IEEE Access*, vol. 8, pp. 47 640–47 653, 2020.

[13] H. Kong, Z. Wen, Y. Jing, and M. Yau, "Midfield over-the-air test: A new ota rf performance test method for 5g massive mimo devices," *IEEE Trans. Microw. Theory Techn.*, vol. 67, no. 7, pp. 2873–2883, 2019.

[14] T. Takahashi, Y. Konishi, and I. Chiba, "A novel amplitude-only measurement method to determine element fields in phased arrays," *IEEE Trans. Antennas Propag.*, vol. 60, no. 7, pp. 3222–3230, 2012.

[15] H. Gao, W. Fan, W. Wang, F. Zhang, Z. Wang, Y. Wu, Y. Liu, and G. F. Pedersen, "On uncertainty investigation of mmwave phased-array element control with an all-on method," *IEEE Antennas Wireless Propag. Lett.*, vol. 19, no. 11, pp. 1993–1997, 2020.

[16] S. D. Silverstein, "Application of orthogonal codes to the calibration of active phased array antennas for communication satellites," *IEEE Trans. Signal Process.*, vol. 45, no. 1, pp. 206–218, 1997.

[17] X. Wei, Y. Jiang, Q. Liu, and X. Wang, "Calibration of phase shifter network for hybrid beamforming in mmwave massive mimo systems," *IEEE Trans. Signal Process.*, vol. 68, pp. 2302–2315, 2020.

[18] S. Mano and T. Katagi, "A method for measuring amplitude and phase of each radiating element of a phased array antenna," *Electronics and Communications in Japan (Part I: Communications)*, vol. 65, no. 5, pp. 58–64, 1982.

[19] C. He, X. Liang, J. Geng, and R. Jin, "Parallel calibration method for phased array with harmonic characteristic analysis," *IEEE Trans. Antennas Propag.*, vol. 62, no. 10, pp. 5029–5036, 2014.

[20] A. O. Fadamiro, A. A.-H. Semomhe, O. J. Famoriji, and F. Lin, "A multiple element calibration algorithm for active phased array antenna," *IEEE J. Multiscale and Multiphys. Comput. Techn.*, vol. 4, pp. 163–170, 2019.

[21] Y.-S. Chen and I.-L. Tsai, "Detection and correction of element failures using a cumulative sum scheme for active phased arrays," *IEEE Access*, vol. 6, pp. 8797–8809, 2018.

[22] T. Takahashi, Y. Konishi, S. Makino, H. Ohmine, and H. Nakaguro, "Fast measurement technique for phased array calibration," *IEEE Trans. Antennas Propag.*, vol. 56, no. 7, pp. 1888–1899, 2008.

[23] W. P. Keizer, "Fast and accurate array calibration using a synthetic array approach," *IEEE Trans. Antennas Propag.*, vol. 59, no. 11, pp. 4115–4122, 2011.

[24] R. Long, J. Ouyang, F. Yang, W. Han, and L. Zhou, "Fast amplitude-only measurement method for phased array calibration," *IEEE Trans. Antennas Propag.*, vol. 65, no. 4, pp. 1815–1822, 2016.

[25] ——, "Multi-element phased array calibration method by solving linear equations," *IEEE Trans. Antennas Propag.*, vol. 65, no. 6, pp. 2931–2939, 2017.

[26] F. Zhang, W. Fan, Z. Wang, Y. Zhang, and G. F. Pedersen, "Improved over-the-air phased array calibration based on measured complex array signals," *IEEE Antennas Wireless Propag. Lett.*, vol. 18, no. 6, pp. 1174–1178, 2019.

[27] T. Nitsche, C. Cordeiro, A. B. Flores, E. W. Knightly, E. Perahia, and J. C. Widmer, "Ieee 802.11 ad: directional 60 ghz communication for multi-gigabit-per-second wi-fi," *IEEE Commun. Mag.*, vol. 52, no. 12, pp. 132–141, 2014.

[28] M. Giordani, M. Polese, A. Roy, D. Castor, and M. Zorzi, "A tutorial on beam management for 3gpp nr at mmwave frequencies," *IEEE Commun. Surveys Tuts.*, vol. 21, no. 1, pp. 173–196, 2018.

[29] L. Berman and A. Feuer, "On perfect conditioning of vandermonde matrices on the unit circle," *The Electronic Journal of Linear Algebra*, vol. 16, 2007.

[30] A. Moitra, "Super-resolution, extremal functions and the condition number of vandermonde matrices," in *Proceedings of the forty-seventh annual ACM symposium on Theory of computing*, 2015, pp. 821–830.

[31] G. Yang, J. Li, D. Wei, and R. Xu, "Study on wide-angle scanning linear phased array antenna," *IEEE Trans. Antennas Propag.*, vol. 66, no. 1, pp. 450–455, 2017.

[32] H. Gao, W. Wang, W. Fan, F. Zhang, Z. Wang, Y. Wu, Y. Liu, and G. F. Pedersen, "Design and experimental validation of automated millimeter-wave phased array antenna-in-package (aip) experimental platform," *IEEE Trans. Instrum. Meas.*, vol. 70, pp. 1–11, 2020.

[33] K. Kibaroglu, M. Sayginer, and G. M. Rebeiz, "A low-cost scalable 32-element 28-ghz phased array transceiver for 5g communication links based on a 2×2 beamformer flip-chip unit cell," *IEEE J. Solid-State Circuits*, vol. 53, no. 5, pp. 1260–1274, 2018.